

Quantum phases of the biased two-chain-coupled Bose-Hubbard ladderJingtao Fan, Xiaofan Zhou ^{*} and Suotang Jia*State Key Laboratory of Quantum Optics and Quantum Optics Devices, Institute of Laser Spectroscopy,
Shanxi University, Taiyuan 030006, China**and Collaborative Innovation Center of Extreme Optics, Shanxi University, Taiyuan 030006, China*

(Received 31 August 2023; accepted 5 January 2024; published 25 January 2024)

We investigate the quantum phases of bosons in a two-chain-coupled ladder. This bosonic ladder is generally in a biased configuration, meaning that the two chains of the ladder can have dramatically different on-site interactions and potential energies. Adopting the numerical density-matrix renormalization-group method, we analyze the phase transitions in various parameter spaces. We find signatures of both insulating-to-superfluid and superfluid-to-insulating quantum phase transitions as the interchain tunneling is increased. Interestingly, tuning the interaction to some intermediate values, the system can exhibit a reentrant quantum phase transition between insulating and superfluid phases. We show that for infinite interaction bias the model is amenable to analytical treatment, predictions of which concerning the phase boundary are in great agreement with numerical results. We finally clarify some critical parameters which separate the system into regimes with distinct phase-transition behaviors, and we briefly compare typical properties of the biased and unbiased bosonic ladder systems. Our paper enriches Bose-Hubbard physics.

DOI: [10.1103/PhysRevA.109.013322](https://doi.org/10.1103/PhysRevA.109.013322)**I. INTRODUCTION**

Strongly correlated bosons, especially those moving in the periodic potentials, have always been a research interest for both experimentalists and theorists, as they are related to a variety of quantum phenomena [1,2]. The simplest model describing such systems is the Bose-Hubbard (BH) model, which incorporates the contributions from the kinetic energy of individual atoms and the repulsive interactions between them [3–12]. Although originally developed in the context of ⁴He liquid [3], it has been demonstrated that the BH model can be feasibly implemented with ultracold atoms trapped in optical lattices [13–16]. Utilizing the unprecedented degree of controllability of the laser fields, all the characteristic parameters of the BH model can be tuned in the optical lattice with high precision [15,16]. Relying on this, the quantum phase transition from a superfluid (SF) to a Mott insulator (MI), which is the most important prediction of the BH model, has been experimentally realized in one [17], two [18], and three dimensions [19]. Since then, lots of related studies have been performed on the extensions of the BH model, by considering, for example, diverse forms of interactions [20–22] and gauge fields [23]. These extensions stimulate the development of new directions bridging condensed-matter physics, stochastic physics, and quantum optics.

In this context, bosons confined to low-dimensional lattices merit special attention, since the correlations built up in these systems are considerably enhanced by the interactions between atoms [24]. Among various low-dimensional lattice models, the two-chain-coupled BH ladder is of

particular importance [25–27], since it serves as an intermediate geometry in one-dimensional (1D) and two-dimensional lattice systems [28]. This provides beneficial insights about the characteristics of the SF-to-MI transition in going from one to two dimensions. As a matter of fact, the BH ladder has been experimentally simulated in different artificial systems [29–31], stimulating immense interests of research towards various aspects of this model, such as chiral currents [29,32–36], quantum magnetism [37–41], and topological states [42–47]. The BH ladders considered in these studies, however, are mostly limited to the symmetric case where both the on-site interactions and potential energies are identical for the two chains. Notice that general ladder systems should also involve the configurations where the two chains have distinctly different system parameters. Actually, letting the two chains of the ladder be asymmetric, with respect to either the interactions or potential energies, may impose major impacts on various properties of the system [48–52]. More importantly, this “biased” ladder structure also underlies the physics behind a large class of systems, such as dressed dipolar molecules [53,54] or Rydberg gases [55–57] in optical lattices and low-dimensional magnetic materials under external fields [58,59].

Motivated by this, in this paper, we investigate the ground-state properties of a biased bosonic ladder at half filling. By saying “biased,” we mean that the two chains constituting the whole ladder can have dramatically different on-site interactions and potential energies. We first provide an analysis of the quantum phases in the limit of infinite interaction bias, where the on-site interaction is infinite for one chain and finite for the other. It is found that, as the interchain tunneling is increased, either the MI-to-SF or the SF-to-MI quantum phase transition can occur depending on the value of

^{*}zhouxiaofan@sxu.edu.cn

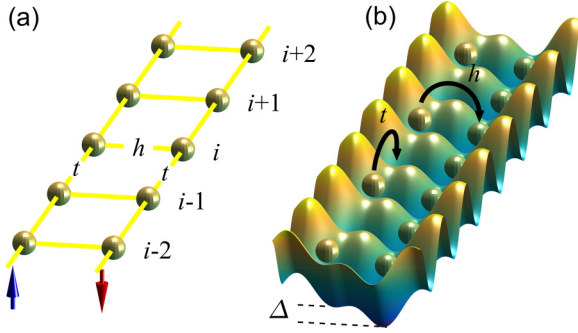


FIG. 1. (a) Schematic picture of the ladder system. The two chains constituting the ladder are designated as spin up and spin down, respectively. The interspin and intraspin hopping amplitudes are denoted, respectively, as t and h . (b) Possible implementation of the bosonic ladder in optical superlattices. The optical double well is generally tilted by an energy difference Δ . The boson tunneling rates along different directions simulate the hopping rates t and h .

interactions. More interestingly, tuning the finite interaction to some intermediate values, the system may even exhibit a reentrant quantum phase transition between MI and SF. By mapping the finite interaction into an effective canonical Kerr nonlinear form, we analytically derive the phase boundary between MI and SF, which agrees well with the numerical results. With the knowledge of the system under infinite interaction bias, we then discuss the more general parameter regime where the interactions of both chains of the ladder are finite. We map out the ground-state phase diagrams in various parameter spaces, and characterize several critical parameters which separate the system into regimes with distinct phase-transition behaviors. Finally, we briefly compare the typical properties of the biased and unbiased bosonic ladder systems.

The numerical calculations in this paper are performed using state-of-the-art density-matrix renormalization-group (DMRG) numerical methods [60,61], with which various physical observables can be precisely obtained. In our numerical simulations, we set the cutoff of the single-site atom number as $n_{\text{cutoff}} = 6$. We set lattice size up to $L = 56$, for which we retain 600 truncated states per DMRG block and perform 20 sweeps with a maximum truncation error of $\approx 10^{-9}$.

II. MODEL AND METHOD

As illustrated in Fig. 1(a), the system in consideration is a bosonic ladder with two coupled chains, which we denote as spin up and spin down, respectively. The interspin tunneling is allowed along the rung. We assume the bosonic ladder is typically biased, i.e., atoms with different spins experience different potential energies and local interactions. Such a scenario can be effectively engineered in spin-dependent optical lattices [62] or optical superlattices [29,63], where the spin index distinguishing different chains can be represented by either the hyperfine sublevels or optical wells, according to different experiment implementations [see Fig. 1(b) for illustration]. The Hamiltonian describing this system reads ($\hbar = 1$

throughout)

$$\hat{H} = -t \sum_{(i,j),\sigma} \hat{b}_{i,\sigma}^\dagger \hat{b}_{j,\sigma} - h \sum_j (\hat{b}_{j,\uparrow}^\dagger \hat{b}_{j,\downarrow} + \text{H.c.}) + \Delta \sum_j (\hat{n}_{j,\uparrow} - \hat{n}_{j,\downarrow}) + \sum_{j,\sigma} \frac{U_\sigma}{2} \hat{n}_{j,\sigma} (\hat{n}_{j,\sigma} - 1) \quad (1)$$

where the field operator $\hat{b}_{j,\sigma}$ ($\hat{b}_{j,\sigma}^\dagger$) annihilates (creates) a bosonic atom with spin σ ($=\uparrow, \downarrow$) at the lattice site j . While atoms with the same spin can hop between adjacent sites $\langle i, j \rangle$ with the intraspin hopping rate t , an interspin field along the rung of the ladder couples atoms with different spins at rate h . The energy bias Δ , which we assume to be positive in this paper, tends to polarize the atoms along the rung of the ladder and U_σ denotes the on-site repulsive interaction of atoms with spin σ ($=\uparrow, \downarrow$). In this paper, we focus on the commensurate ladder with total atomic density $\rho = N/2L = 1/2$. Here, $N = N_\uparrow + N_\downarrow$ is the total number of bosons on the two-chain ladder, each of which has length L . This amounts to setting the total system size to be $2L$. In the following discussion, we set the energy scale by taking $t = 1$, and we also take $\Delta = 10$ unless otherwise specified.

The Hamiltonian (1) can be viewed as a natural extension of the single-component 1D BH model incorporating the spin degree of freedom, which is controlled by both the transverse and longitude magnetic fields. Without the interspin tunneling h , the ladder decouples and reduces to two independent BH chains. A finite energy bias Δ (>0) then polarizes the bosons to the spin-down chain with commensurability of one boson per site, leaving the spin-up chain empty. In this case, the physics is entirely governed by the usual 1D BH model, which has been extensively explored [3–8]. With a nonzero interspin tunneling h , however, the two BH chains are coupled together, meaning that the characteristic parameters of each individual chain may impact the ground-state properties of the composite system in a collective manner. This becomes especially interesting if the on-site interactions of the two chains are tuned quite different. Without loss of generality, let us assume $U_\uparrow > U_\downarrow$ and take a preanalysis on the behavior of the BH chain with spin down. In this case, the on-site interaction may be effectively enhanced through a high-order tunneling process triggered by h [64], favoring the formation of MI, whereas the particle filling factor may deviate from unity at the same time, which in turn promotes the SF behavior. The seemingly opposite tendency of the ground-state property makes the roles of the parameters in the biased bosonic ladder less intuitive and to be quantitatively clarified.

The MI and SF phases can be directly identified by calculating the charge gap δ_L , defined as the difference between the energies needed to add and remove one particle from the system, i.e.,

$$\delta_L = \mu_L^+ - \mu_L^-, \quad (2)$$

$$\mu_L^+ = E_L(N+1) - E_L(N), \quad (3)$$

$$\mu_L^- = E_L(N) - E_L(N-1), \quad (4)$$

where $E_L(N)$ is the the ground-state energy for L sites and N particles, and the chemical potentials μ_L^+ and μ_L^- characterize

the energy cost to add and remove one particle, respectively. The insulating phase is signaled by the opening up of δ_L in the thermodynamic limit $N, L \rightarrow \infty$ with fixed density ρ , consistent with the zero compressibility $\kappa (= \partial\rho/\partial\mu)$ of an insulator [65]. In the SF phase, however, the charge gap δ_L closes and the system becomes compressible in the thermodynamic limit.

Since δ_L keeps finite for any finite systems, in order to pinpoint the MI-to-SF transition in the parameter space, we should extrapolate to the $L \rightarrow \infty$ limit by utilizing proper finite-size scaling. Notice that the transition between MI and SF phases at commensurate fillings is shown to be of Berezinskii-Kosterlitz-Thouless type [25,26,48], around which the charge gap closes exponentially as $\delta \sim \exp(-b/\sqrt{U_\sigma - U_c})$ where b is a constant. To precisely determine the transition point, in the critical region, one may employ the following finite-size-scaling relation for the charge gap [10,66]:

$$L\delta_L \times \left(1 + \frac{1}{2 \ln L + C}\right) = F\left(\frac{\xi}{L}\right) \quad (5)$$

where F is a scaling function, C is an unknown constant to be determined, and ξ is the correlation length which is related to the charge gap at the critical point as $\xi \sim \delta^{-1}$. The scaling function F turns out to be system size independent in the SF region because of the divergence of the correlation length. Hence, plots of the rescaled gap $L\delta_L^* = L\delta_L[1 + 1/(2 \ln L + C)]$ as function of ξ/L for different values of L and U_σ should collapse onto a unique curve representing F . This provides a formal approach to obtain the parameters b , C , and U_c . For the single-component 1D BH model, the best collapse of the data for $L\delta_L^*$ versus ξ/L occurs at $C \rightarrow \infty$ [10], and we have numerically checked that the latter still holds for the present model with finite h . We then immediately have $\delta_L = \delta_L^*$, indicating that in the SF region $L\delta_L$ should not change with varying system size L (i.e., δ_L vanishes linearly as the system size increases to infinity). In other words, in the critical region, we can safely extrapolate the charge gap to the thermodynamic limit with satisfactory accuracy by fitting it to a linear function in terms of $1/L$.

III. RESULTS

In the following, we systematically study the ground-state properties of the biased bosonic ladder. Before providing the results of general parameters, we first put the interaction bias to infinity, i.e., we consider the bosonic ladder consisting of one chain with infinite on-site interaction and the other with finite on-site interaction. The physics in this limit serves as a beneficial starting point to understand the essential mechanism behind different kinds of phase transitions.

A. Infinite interaction bias: $U_\uparrow - U_\downarrow = \infty$

Without loss of generality, we fix the on-site interaction of the spin-up BH chain to be infinity, $U_\uparrow \rightarrow \infty$, and that of the spin-down chain to be finite. This amounts to imposing a hard-core constraint on each site of the spin-up chains, where only one boson is allowed to occupy.

Before showing the full phase diagram, we can gain some useful insights into the system by inspecting certain limits.

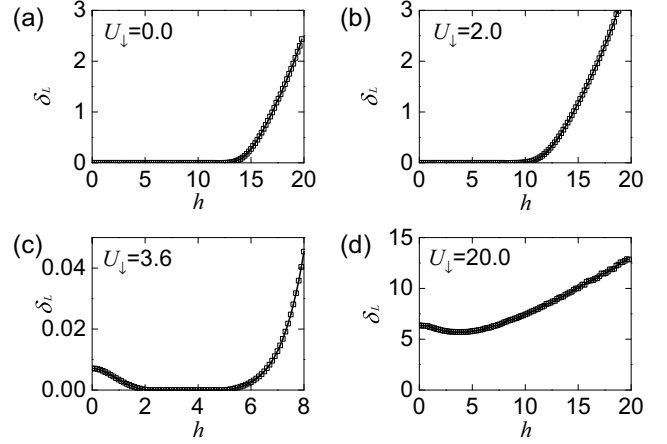


FIG. 2. The charge gap δ_L , extrapolated to $L \rightarrow \infty$, as a function of h with (a) $U_\downarrow = 0.0$, (b) $U_\downarrow = 2.0$, (c) $U_\downarrow = 3.6$, and (d) $U_\downarrow = 20.0$. The other parameters are $\Delta = 10$ and $U_\uparrow = \infty$.

As mentioned in Sec. II, the simplest limit is the zero interspin tunneling $h = 0$, under which the ground state is fully described by the 1D BH model with unit filling. It is well known that the 1D BH model with unit filling shows a SF-to-MI transition at $U_c/t \approx 3.3$ [6–12]. The physics becomes richer when h is turned on. In this case, if we further set the on-site interaction U_\downarrow to be zero, the system closely resembles that of two-level atoms inside cavity arrays for which the Jaynes-Cummings-Hubbard (JCH) model works [67–70]. This can be seen clearly if we map the field operators of the hardcore bosons to those of quantum spins by $\hat{b}_{j,\uparrow} \rightarrow \sigma_-$ and $\hat{b}_{j,\uparrow}^\dagger \rightarrow \sigma_+$, where σ_- and σ_+ are spin-1/2 lowering and raising operators, respectively. Therefore, the Hamiltonian describing the tunneling process between the two BH chains becomes Jaynes-Cummings type, in which the spin-down bosons act as interaction-free photons bridging adjacent lattice sites. It follows directly from the JCH physics that, by increasing h , the spin-down bosons behave more localized and consequently undergo a phase transition from SF to MI at some critical tunneling strength h_c [67,68].

Another interesting limit which is opposite to the JCH regime is $U_\downarrow \rightarrow \infty$, implying a hard-core constraint on both chains. It has been analytically demonstrated that, for the symmetric hard-core BH ladder with $\Delta = 0$, the critical tunneling strength h_c decreases down to zero [71]. As a finite energy bias Δ usually tends to increase the band gap, we expect the system keeps insulating irrespective of the specific value of h .

We now start to show the numerical results of general parameters. In order to clarify the effect of the interspin tunneling on the SF-to-MI transition, we vary h from zero to some large value and calculate the corresponding charge gap δ_L , which ought to be extrapolated to the $L \rightarrow \infty$ limit. From the knowledge of the 1D BH model, the system stays at the SF phase (MI phase) for $U_\downarrow \lesssim 3.3$ ($U_\downarrow \gtrsim 3.3$) and $h = 0$, and potential phase transitions can take place when increasing h . Figure 2(a) plots the charge gap δ_L as a function of h for $U_\downarrow = 0$. It can be seen that, starting from zero, the charge gap gradually opens up when h exceeds the critical value $h_c = 12.5(1)$, evidencing a SF-to-MI transition, as can

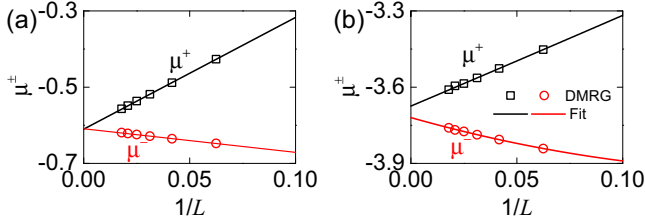


FIG. 3. The finite-size scaling of chemical potentials μ_L^+ and μ_L^- for (a) $h = 3.0$ and (b) $h = 8.0$. The other parameters are $\Delta = 10$, $U_\downarrow = 3.6$, and $U_\uparrow = \infty$.

be inferred from the JCH physics [68]. The critical tunneling strength h_c decreases as we increase the on-site interaction U_\downarrow , as shown in Fig. 2(b). In Fig. 2(d), we exemplify another limit where the on-site interaction is considerably strong by setting $U_\downarrow = 20$. It can be found that, in this case, the gap δ_L stays open irrespective of the value of h , meaning the system remains a MI. Something interesting happens when the on-site interaction U_\downarrow is tuned slightly larger than U_c . As illustrated in Fig. 2(c), we plot δ_L versus h for $U_\downarrow = 3.6$. With the increase of h , the gap first closes at $h = 2.0(1)$ and then reopens at $h = 5.1(1)$, indicating that the phase transition appears twice. That is, the system starts from the MI, and subsequently traverses the SF phase, ending up in the MI eventually. Figures 3(a) and 3(b) show finite-size scaling of the DMRG data of the charge gap, by linear and quadratic fittings, for two representative points located in the SF and MI phases, respectively. This reentrant MI phase transition induced by the interspin tunneling strength h does not exist in the symmetric bosonic ladder with $U_\uparrow = U_\downarrow$ and $\Delta = 0$, and is thus exclusive for the biased ladder here.

With the understanding above, we map out the phase diagram in the U_\downarrow - h plane in Fig. 4. The phase boundary has

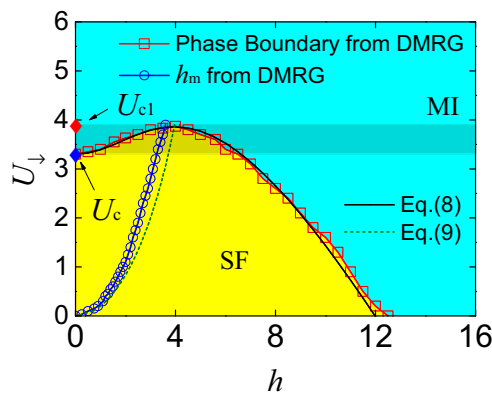


FIG. 4. The phase diagram in the U_\downarrow - h plane for $\Delta = 10$ and $U_\uparrow = \infty$. The red solid line with square symbol (black solid line) denotes The MI-SF phase boundary obtained by the DMRG calculation [Eq. (8)]. The values of h_m (i.e., the location of the maximum of the CF; see the main text) for each U_\downarrow are also pinpointed in the phase diagram by the blue solid line with circle symbol. For comparison, location of the minimum of U_{eff} , determined by Eq. (9), is plotted by the green dashed line. The shaded area, bounded by critical interactions $U_c = 3.30(2)$ and $U_{c1} = 3.91(2)$, characterizes the parameter region where the MI-to-SF-to-MI transition can occur.

been extrapolated to the $L \rightarrow \infty$ limit by the finite-size scaling. It is to be seen clearly that, while increasing the on-site interaction U_\downarrow always drives the system to the MI phase, the role of the interspin tunneling h can be somehow opposite, i.e., it can trigger both the MI and SF phases, depending on the value of U_\downarrow . Notice that the MI in the BH model is essentially stabilized by the direct interaction between bosons, whereas bosons with different spins are dressed together here, forming composite polaritons. We therefore expect that some effective interaction between polaritons, which plays the key role of inducing different behaviors of the phase transition, may emerge.

To see this clearly, we map the local contribution of the Hamiltonian (1) into an effective Kerr nonlinearity by a simple energy mismatch argument. As detailed in Appendix A, the local energy of Hamiltonian (1) consists of two polaritonic modes the eigenenergies of which are

$$\omega_n^\pm = \frac{U_\downarrow}{2}n(n-2) + \frac{1}{2}(\Delta + U_\downarrow) \pm \frac{1}{2}\sqrt{(nU_\downarrow - U_\downarrow - \Delta)^2 + 4nh^2} \quad (6)$$

where n is the excitation number. Since we are only interested in the low-energy physics, the focus in the following will be on the lower branch ω_n^- . We define the effective Hubbard interaction U_{eff} as the energy cost incurred by forming a two-particle polaritonic excitation (with energy ω_2^-) from two single-particle polaritonic excitations (with energy $2\omega_1^-$) in neighboring lattice sites [69,70], i.e.,

$$\begin{aligned} U_{\text{eff}} &= \omega_2^- - 2\omega_1^- \\ &= \frac{1}{2}(U_\downarrow - \Delta) + \sqrt{\Delta^2 + 4h^2} \\ &\quad - \frac{\sqrt{(U_\downarrow - \Delta)^2 + 8h^2}}{2}. \end{aligned} \quad (7)$$

With this understanding, we can obtain an analytical expression of the phase boundary between the MI and SF phases by equating the effective interaction U_{eff} with the critical interaction strength of the 1D BH model with unit filling, namely,

$$U_{\text{eff}} = U_c = 3.3. \quad (8)$$

As shown in Fig. 4, the curve defined by Eq. (8) agrees well with the numerical results obtained by the DMRG calculation. It should be emphasized that, in deriving Eq. (7), we have implicitly assumed that the ground-state property of the whole lattice system is mainly governed by its low-energy local physics. This requires that (i) the energy scale owned by each local lattice site is considerably larger than the kinetic energy of bosons, namely, at least $\Delta \gg 1$ or $h \gg 1$, and (ii) the density fluctuations are weak enough so that only the lowest-lying excitations of individual lattice sites need to be taken into consideration. This guarantees the effectiveness of Eq. (8) in predicting the MI-to-SF phase boundary, since the density fluctuations are extremely suppressed in the MI. Equation (7) provides further guidance to the driving force inducing different phase transitions. An interesting finding is that U_{eff} exhibits nonmonotonic behavior as h increases from zero. As illustrated in Fig. 5(a), with the increase of h , the effective interaction U_{eff} decreases first to a minimum and

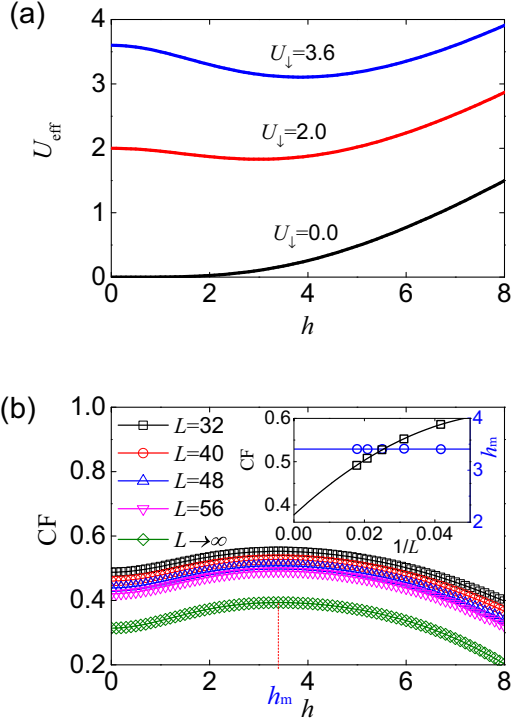


FIG. 5. (a) The effective Hubbard interaction U_{eff} as a function of h for different U_{\downarrow} with $\Delta = 10$ and $U_{\uparrow} = \infty$. (b) The CF calculated for different system sizes. Note that the result of $L \rightarrow \infty$ is obtained by extrapolation using the finite-size scaling. h_m specifies the location of the maximum of the CF. The inset shows the finite-size scaling of h_m (blue symbols and line) and the CF at $h = 3.4$ (black symbols and line). It is shown that h_m does not change with the system size. The other parameters are $\Delta = 10$, $U_{\downarrow} = 3.6$, and $U_{\uparrow} = \infty$.

then increases monotonically [see blue line], which explains the MI-to-SF-to-MI transition found in Fig. 4. The location of the minimum of U_{eff} can be easily deduced by requiring $\partial U_{\text{eff}}/\partial h = 0$, yielding a trivial solution $h = 0$ and a nontrivial solution:

$$h = \frac{\sqrt{\Delta^2 - (\Delta - U_{\downarrow})^2}}{2}. \quad (9)$$

It is straightforward to show that Eq. (9), within its range of values, minimizes U_{eff} . The curve obtained from Eq. (9) is depicted in Fig. 4. Notice that, whereas U_{eff} is minimized by $h = 0$ when $U_{\downarrow} = 0$, consistent with the JCH physics [67,68], a nonzero U_{\downarrow} shifts the location of the interaction minimum (i.e., $h = 0$) to some finite value. Within this picture, an upper bound of U_{\downarrow} , beyond which no SF phase would exist, can be obtained. This is immediately achieved by substituting Eq. (9) into Eq. (8), which is then solved by

$$U_{\downarrow} = U_{c1} \equiv \Delta + U_c - \sqrt{\Delta^2 - U_c^2}. \quad (10)$$

It becomes clear that the parameter region of U_{\downarrow} within which the MI-to-SF-to-MI transition can occur is $U_c < U_{\downarrow} < U_{c1}$.

An experimental measurable quantity that is able to mirror the effective interaction is the condensate fraction (CF), defined as the number of bosons in the condensate with respect to the total number of bosons [65,72]. It has been shown

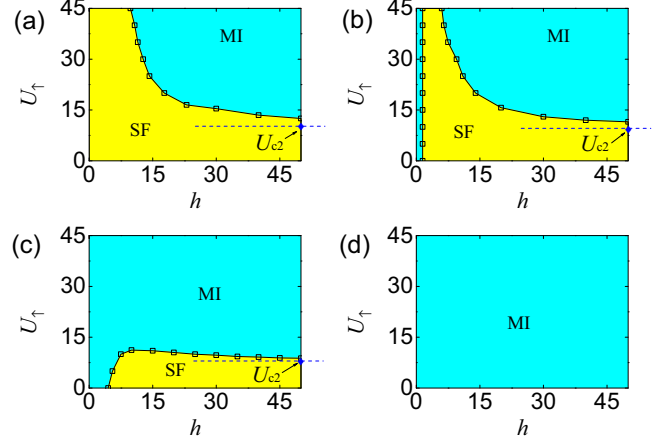


FIG. 6. The phase diagram in the U_{\uparrow} - h plane with $\Delta = 10$ and (a) $U_{\downarrow} = 3.0$, (b) $U_{\downarrow} = 3.6$, (c) $U_{\downarrow} = 5.0$, and (d) $U_{\downarrow} = 15.0$.

that the condensate fraction of Bose gases monotonically decreases as the local interaction increases [65]. For the bosonic ladder considered here, the CF is defined as the largest eigenvalue of the matrix $\langle \hat{b}_{i,\sigma}^{\dagger} \hat{b}_{j,\sigma'} \rangle$ divided by the total number of bosons [72]. Figure 5(b) shows the CF as a function of h for $U_{\downarrow} = 3.6$ and different system sizes. The values of $L \rightarrow \infty$ are obtained by the standard finite-size scaling [the inset of Fig. 5(b)]. It is demonstrated that the CF increases first, reaching its maximum at $h = 3.4(1)$, and then decreases. The location of the maximum of CF, designated as h_m , depends sensitively on the value of U_{\downarrow} . As shown in Fig. 4, we plot h_m for varying U_{\downarrow} , which exhibits the same behavior as that obtained from Eq. (9). The agreement between h_m and Eq. (9) signals that the picture of the effective interaction U_{eff} works in a wide range of parameters, even inside the SF phase where the density fluctuation is somehow enhanced.

B. Finite interaction bias: $U_{\uparrow} - U_{\downarrow} < \infty$

Having understood the physics of the bosonic ladder under infinite interaction bias, we are now in the stage to explore the more general parameter regime where the interactions of both chains of the ladder are finite. Here we are particularly interested in the influence of finite spin-up interaction on various quantum phases. By calculating the charge gap δ_L with extrapolation to the thermodynamic limit, we obtain the phase diagrams in the U_{\uparrow} - h plane in Figs. 6(a)–6(d) with different U_{\downarrow} . As shown in Fig. 6(a), in which the spin-down interaction is fixed as $U_{\downarrow} = 3.0$ ($< U_c$), the SF region is confined by a smooth phase boundary, which extends up to $U_{\uparrow} \rightarrow \infty$ and $h \rightarrow \infty$. A phase transition from the SF to MI may occur when increasing U_{\uparrow} (h) for some fixed h (U_{\uparrow}). Increasing the spin-down interaction slightly larger than U_c , for example $U_{\downarrow} = 3.6$, the MI can emerge for small h , penetrating the SF region, as illustrated in Fig. 6(b). Importantly, as h approaches infinity, the spin-up interaction delimiting different quantum phases decreases and saturates to some critical value U_{c2} .

In fact, through an analysis of the polaritonic modes, the MI-to-SF phase boundary in the $h \rightarrow \infty$ limit can be derived as $U_{\uparrow} + U_{\downarrow} = 4U_c \approx 13.2$ (see Appendix B for details). Setting $U_{\uparrow} = U_{\downarrow} = U$, we immediately reproduce the result

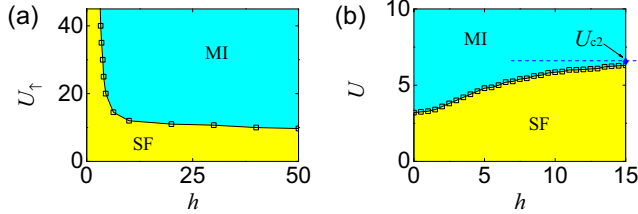


FIG. 7. (a) The phase diagram in the U_{\uparrow} - h plane with $U_{\downarrow} = 3.6$ and $\Delta = 0$. (b) The phase diagram in the U - h plane with $U = U_{\uparrow} = U_{\downarrow}$ and $\Delta = 10$.

of the symmetric case, i.e., $U = 2U_c \approx 6.6$, obtained by the bosonization method [26]. Under this framework, the critical interaction U_{c2} is straightforwardly written as

$$U_{c2} = 4U_c - U_{\downarrow}. \quad (11)$$

As marked in Fig. 6(b) by blue dashed line, the critical interaction U_{c2} defined above separates the phase diagram into two distinct parameter regimes. For the $U_{\uparrow} > U_{c2}$ side, there may exist the interesting MI-to-SF-to-MI phase transition we explored in Sec. III A, whereas for $U_{\uparrow} < U_{c2}$, the MI-to-SF phase transition can appear only once by monotonically varying h .

Adopting the description of the effective interaction introduced in Sec. III A, we anticipate that if U_{\downarrow} is increased to be larger than U_{c1} , a finite upper bound of U_{\uparrow} , beyond which the SF phase disappears, can emerge. This is confirmed by the phase diagram in Fig. 6(c), where we take $U_{\downarrow} = 5$ [$> U_{c1} = 3.91(2)$]. As expected, the SF phase is destroyed for $U_{\uparrow} \gtrsim 11$, in contrast to the behavior shown in Figs. 6(a) and 6(b). Increasing U_{\downarrow} further such that $U_{\downarrow} > 4U_c$, the critical interaction U_{c2} touches zero, meaning that the SF disappears, at least when h is sufficiently large. The phase diagram with $U_{\downarrow} = 15$ ($> 4U_c$) is plotted in Fig. 6(d), from which we find that the area of SF completely vanishes.

Up to now, our focus has been basically on the parameter regime where both the interactions and potential energies of the two chains are asymmetric. The individual effect incurred by one of the two asymmetric ingredients, i.e., either the interaction asymmetry or the potential energy asymmetry, has not been elucidated. Here we complement this study by plotting two additional phase diagrams, each of which has only one asymmetric ingredient. The phase diagram in the U_{\uparrow} - h plane with zero energy bias ($\Delta = 0$) and fixed spin-down interaction ($U_{\downarrow} = 3.6$) is plotted in Fig. 7(a). The phase diagram in this case shares the same structure with that in Fig. 6(a), albeit with shrunken SF area. It is also understood that no MI phase can be found for sufficiently small h , contrasting the behavior in Fig. 6(b), since a zero Δ always closes the charge gap for lattices with noninteger filling at $h = 0$. As shown in Fig. 7(b), by requiring the interactions of the two chains to be equal, setting $U = U_{\uparrow} = U_{\downarrow}$, we map the phase diagram in the U - h plane with finite energy bias $\Delta = 10$. With the increase of h , the critical interaction of the SF-to-MI transition monotonically increases, asymptotically up to $U_{c2} = 6.60(4)$, showing a distinct behavior compared to cases with asymmetric interactions.

IV. DISCUSSION AND CONCLUSION

We first briefly discuss the precision of the transition points located in the obtained phase diagrams. For $h = 0$, our model reduces to the usual 1D BH model with unit filling, the transition point U_c of which has been obtained through widely different techniques with considerably high precision [6–12]. Our DMRG calculation accompanied with a linear finite-size scaling of the gap in the critical region produces $U_c = 3.30(2)$ (see Fig. 4 and caption). The obtained U_c here is in great agreement with the recent estimations [e.g. $U_c = 3.279(1)$ in Ref. [10] and $U_c = 3.311(1)$ in Refs. [11,12]]. As mentioned at the end of Sec. II, the linear scaling relation in the critical region extends to regimes with $h \neq 0$, and we therefore expect the transition points obtained in the whole phase diagram can reach sufficiently high precision.

As mentioned in Sec. II, the considered model can be directly implemented with ultracold atoms inside optical lattices under various experiment designs. For example, the bosonic ladder can be prepared by growing optical superlattices, which form a double-well structure along one direction [29,63]. The tunneling strength h , on-site interactions $U_{\uparrow/\downarrow}$, and energy bias Δ can be independently controlled by properly tuning the geometry of the optical double well. Alternatively, one can employ spin-dependent optical lattices [62], where atoms with different hyperfine states experience different lattice potentials. In this scenario, Δ and h are respectively controlled by the detuning and Rabi frequency of an additional coupling laser, and the on-site interactions $U_{\uparrow/\downarrow}$ can be tuned via Feshbach resonances or the lattice depths experienced by atoms with different spins. In spite of the research interests in the model in its own right, our results offer beneficial insights into engineering effective interactions on demand by dressing different atomic internal states [55,64]. That said, our model constitutes only a subset of the rich physics in the BH ladder with coupled chains, and many interesting extensions are to be applied in the future. For example, with a ladder structure, the hopping process of atoms may carry nontrivial Peierls phases, giving rise to synthetic gauge fields [73]. These gauge fields may not only affect the MI-to-SF transitions dramatically [23] but also induce various chiral currents [29,32–36]. Another direction is to fit the system into the grand-canonical description by introducing a tunable chemical potential [3,48]. This may provide new perspectives on the magnetic or charge correlations in Mott lobes with different filling factors.

In conclusion, we have theoretically studied the ground-state properties of the BH ladder with half filling in a biased configuration by using state-of-the-art DMRG numerical methods. It is found that the interchain tunneling can drive both the MI-to-SF and SF-to-MI quantum phase transitions, depending on the value of interactions. A reentrant quantum phase transition between MI and SF has also been predicted by setting the on-site interactions to intermediate values. Under appropriate conditions, the model is shown to be amenable to analytical treatment, predictions of which concerning the phase boundary are in great agreement with numerical results. Armed with this knowledge, we have mapped out the full phase diagram and characterized some critical parameters, separating the system into regimes with distinct phase-transition behaviors.

ACKNOWLEDGMENTS

This work is supported by the National Key Research and Development Program of China under Grant No. 2022YFA1404003; the National Natural Science Foundation of China under Grants No. 12004230, No. 12174233, and No. 12034012; and the Research Project Supported by Shanxi Scholarship Council of China and Shanxi under Grant No. 1331KSC.

APPENDIX A: POLARITONIC MODES OF THE LOCAL HAMILTONIAN

In this Appendix, we derive Eq. (6) in the main text. To that end, we rearrange the Hamiltonian (1) as

$$\hat{H} = \sum_j \hat{H}_L^{(j)} - t \sum_{\langle i,j \rangle, \sigma} \hat{b}_{i,\sigma}^\dagger \hat{b}_{j,\sigma} \quad (\text{A1})$$

where

$$\begin{aligned} \hat{H}_L^{(j)} = & -h(\hat{b}_\uparrow^\dagger \hat{b}_\downarrow + \text{H.c.}) + \Delta(\hat{n}_\uparrow - \hat{n}_\downarrow) \\ & + \sum_\sigma \frac{U_\sigma}{2} \hat{n}_\sigma (\hat{n}_\sigma - 1) \end{aligned} \quad (\text{A2})$$

describes the local physics at lattice site j . Note that we have omitted the subscript j in the right-hand side of Eq. (A2) for simplicity. The Hamiltonian (A2) can be spanned by the Fock basis $|n_\downarrow, n_\uparrow\rangle$, where \hat{n}_σ is the occupation number for bosons with spin σ (\uparrow, \downarrow). In the $U_\uparrow \rightarrow \infty$ limit, a hardcore constraint on the spin-up bosons can be imposed, meaning that we only need to retain the states $|n, 0\rangle$ and $|n-1, 1\rangle$ with the total occupation $n = n_\downarrow + n_\uparrow$. The polaritonic modes of Hamiltonian (A2) are therefore admixtures of $|n, 0\rangle$ and $|n-1, 1\rangle$, and the eigenenergies are readily diagonalized as

$$\begin{aligned} \omega_n^\pm = & \frac{U_\downarrow}{2} n(n-2) + \frac{1}{2}(\Delta + U_\downarrow) \\ & \pm \frac{1}{2} \sqrt{(nU_\downarrow - U_\downarrow - \Delta)^2 + 4nh^2}. \end{aligned} \quad (\text{A3})$$

APPENDIX B: EFFECTIVE LOW-ENERGY DESCRIPTION IN THE $h \rightarrow \infty$ LIMIT

Here we provide an effective low-energy description of the model in the $h \rightarrow \infty$ limit. We first introduce two branches of quasimodes $\hat{b}_{j,+}$ and $\hat{b}_{j,-}$ defined as

$$\hat{b}_{j,+} = \frac{1}{\sqrt{2}}(\hat{b}_{j,\uparrow} + \hat{b}_{j,\downarrow}), \quad (\text{B1})$$

$$\hat{b}_{j,-} = \frac{1}{\sqrt{2}}(\hat{b}_{j,\uparrow} - \hat{b}_{j,\downarrow}). \quad (\text{B2})$$

Under the transformations of Eqs. (B1) and (B2), the Hamiltonian (1) is rewritten as

$$\hat{H} = \sum_j \hat{H}_L^{(j)} - t \sum_{\langle i,j \rangle} (\hat{b}_{i,+}^\dagger \hat{b}_{j,+} + \hat{b}_{i,-}^\dagger \hat{b}_{j,-}) \quad (\text{B3})$$

where the local Hamiltonian reads

$$\begin{aligned} \hat{H}_L^{(j)} = & \left(\frac{U_\downarrow}{8} + \frac{U_\uparrow}{8} \right) [(\hat{n}_{j,+} + \hat{n}_{j,-})^2 + (\hat{b}_{j,+}^\dagger \hat{b}_{j,-} + \hat{b}_{j,-}^\dagger \hat{b}_{j,+})^2 \\ & - 2(\hat{n}_{j,+} + \hat{n}_{j,-})] + \left(\frac{U_\downarrow}{4} - \frac{U_\uparrow}{4} \right) [(\hat{b}_{j,+}^\dagger \hat{b}_{j,-} \\ & + \hat{b}_{j,-}^\dagger \hat{b}_{j,+})(\hat{n}_{j,+} + \hat{n}_{j,-} - 1)] + \frac{\Delta}{2} (\hat{n}_{j,+} + \hat{n}_{j,-} \\ & - \hat{b}_{j,+}^\dagger \hat{b}_{j,-} - \hat{b}_{j,-}^\dagger \hat{b}_{j,+}) + h(\hat{n}_{j,+} - \hat{n}_{j,-}). \end{aligned} \quad (\text{B4})$$

It follows from Eq. (B4) that the low-energy physics is dominated by bosons on the “-” polaritonic branch in the $h \rightarrow \infty$ limit. We thus anticipate an effective low-energy theory which is purely described by field operators of the “-” polaritonic branch. The simplest way to achieve this is to average the Hamiltonian (B3) with respect to the vacuum state of the “+” polaritonic branch, yielding

$$\begin{aligned} \hat{H}_{\text{eff}} = & \sum_j \left[\left(\frac{\Delta}{2} - h \right) \hat{n}_{j,-} + \frac{\tilde{U}}{2} \hat{n}_{j,-} (\hat{n}_{j,-} - 1) \right] \\ & - t \sum_{\langle i,j \rangle} \hat{b}_{i,-}^\dagger \hat{b}_{j,-} \end{aligned} \quad (\text{B5})$$

where $\tilde{U} = (U_\downarrow + U_\uparrow)/4$. Notice that the effective description in the Hamiltonian (B5) becomes accurate when h approaches infinity. More importantly, the Hamiltonian (B5) is written in the same form of the 1D BH model with effective on-site interaction \tilde{U} . It follows that the physics of our ladder system in this limit can be effectively described by the 1D BH model with simple substitution of system parameters. Given this, the SF-to-MI phase boundary is readily obtained as $\tilde{U} = U_c \approx 3.3$.

- [1] F. Dalfovo, S. Giorgini, L. P. Pitaevskii, and S. Stringari, Theory of Bose-Einstein condensation in trapped gases, *Rev. Mod. Phys.* **71**, 463 (1999).
- [2] C. Orzel, A. K. Tuchman, M. L. Fenselau, M. Yasuda, and M. A. Kasevich, Squeezed states in a Bose-Einstein Condensate, *Science* **291**, 2386 (2001).
- [3] M. P. A. Fisher, P. B. Weichman, G. Grinstein, and D. S. Fisher, Boson localization and the superfluid-insulator transition, *Phys. Rev. B* **40**, 546 (1989).

- [4] W. Krauth, M. Caffarel, and J.-P. Bouchaud, Gutzwiller wave function for a model of strongly interacting bosons, *Phys. Rev. B* **45**, 3137 (1992).
- [5] A. P. Kampf and G. T. Zimanyi, Superconductor-insulator phase transition in the boson Hubbard model, *Phys. Rev. B* **47**, 279 (1993).
- [6] J. K. Freericks and H. Monien, Strong-coupling expansions for the pure and disordered Bose-Hubbard model, *Phys. Rev. B* **53**, 2691 (1996).

- [7] V. A. Kashurnikov and B. V. Svistunov, Exact diagonalization plus renormalization-group theory: Accurate method for a one-dimensional superfluid-insulator-transition study, *Phys. Rev. B* **53**, 11776 (1996).
- [8] T. D. Kühner and H. Monien, Phases of the one-dimensional Bose-Hubbard model, *Phys. Rev. B* **58**, R14741 (1998).
- [9] S. Ejima, H. Fehske and F. Gebhard, Dynamic properties of the one-dimensional Bose-Hubbard model, *Europhys. Lett.* **93**, 30002 (2011).
- [10] J. Carrasquilla, S. R. Manmana, and M. Rigol, Scaling of the gap, fidelity susceptibility, and Bloch oscillations across the superfluid-to-Mott-insulator transition in the one-dimensional Bose-Hubbard model, *Phys. Rev. A* **87**, 043606 (2013).
- [11] J. Arcila-Forero, R. Franco, and J. Silva-Valencia, Critical points of the anyon-Hubbard model, *Phys. Rev. A* **94**, 013611 (2016).
- [12] Z. Zuo, S. Yin, X. Cao, and F. Zhong, Scaling theory of the Kosterlitz-Thouless phase transition, *Phys. Rev. B* **104**, 214108 (2021).
- [13] M. Lewenstein, A. Sanpera, and V. Ahufinger, *Ultracold Atoms in Optical Lattices* (Oxford University, London, 2012).
- [14] D. Jaksch, C. Bruder, J. I. Cirac, C. W. Gardiner, and P. Zoller, Cold bosonic atoms in optical lattices, *Phys. Rev. Lett.* **81**, 3108 (1998).
- [15] E. Demler and F. Zhou, Spinor Bosonic atoms in optical lattices: Symmetry breaking and fractionalization, *Phys. Rev. Lett.* **88**, 163001 (2002).
- [16] I. Bloch, J. Dalibard, and W. Zwerger, Many-body physics with ultracold gases, *Rev. Mod. Phys.* **80**, 885 (2008).
- [17] T. Stöferle, H. Moritz, C. Schori, M. Köhl, and T. Esslinger, Transition from a strongly interacting 1D superfluid to a mott insulator, *Phys. Rev. Lett.* **92**, 130403 (2004).
- [18] I. B. Spielman, W. D. Phillips, and J. V. Porto, Mott-insulator transition in a two-dimensional atomic Bose gas, *Phys. Rev. Lett.* **98**, 080404 (2007).
- [19] M. Greiner, O. Mandel, T. Esslinger, T. W. Hänsch and I. Bloch, Quantum phase transition from a superfluid to a Mott insulator in a gas of ultracold atoms, *Nature (London)* **415**, 39 (2002).
- [20] A. Kuklov, N. Prokof'ev, and B. Svistunov, Commensurate two-component bosons in an optical lattice: Ground state phase diagram, *Phys. Rev. Lett.* **92**, 050402 (2004).
- [21] V. W. Scarola and S. Das Sarma, Quantum phases of the extended Bose-Hubbard Hamiltonian: Possibility of a supersolid state of cold atoms in optical lattices, *Phys. Rev. Lett.* **95**, 033003 (2005).
- [22] O. Mansikkamäki, S. Laine, and M. Silveri, Phases of the disordered Bose-Hubbard model with attractive interactions, *Phys. Rev. B* **103**, L220202 (2021).
- [23] R. Sachdeva, M. Singh, and T. Busch, Extended Bose-Hubbard model for two-leg ladder systems in artificial magnetic fields, *Phys. Rev. A* **95**, 063601 (2017).
- [24] M. A. Cazalilla, R. Citro, T. Giamarchi, E. Orignac, and M. Rigol, One dimensional bosons: From condensed matter systems to ultracold gases, *Rev. Mod. Phys.* **83**, 1405 (2011).
- [25] E. Orignac and T. Giamarchi, Vortices in coupled planes with columnar disorder and bosonic ladders, *Phys. Rev. B* **57**, 11713 (1998).
- [26] P. Donohue and T. Giamarchi, Mott-superfluid transition in bosonic ladders, *Phys. Rev. B* **63**, 180508(R) (2001).
- [27] M. S. Luthra, T. Mishra, R. V. Pai, and B. P. Das, Phase diagram of a bosonic ladder with two coupled chains, *Phys. Rev. B* **78**, 165104 (2008).
- [28] E. Dagotto and T. M. Rice, Surprises on the way from one- to two-dimensional quantum magnets: The ladder materials, *Science* **271**, 618 (1996).
- [29] M. Atala, M. Aidelsburger, Mi. Lohse, J. T. Barreiro, B. Paredes and I. Bloch, Observation of chiral currents with ultracold atoms in bosonic ladders, *Nat. Phys.* **10**, 588 (2014).
- [30] S. Greschner, M. Piraud, F. Heidrich-Meisner, I. P. McCulloch, U. Schollwöck, and T. Vekua, Spontaneous increase of magnetic flux and chiral-current reversal in bosonic ladders: Swimming against the tide, *Phys. Rev. Lett.* **115**, 190402 (2015).
- [31] Q. Zhu, Z.-H. Sun, M. Gong, F. Chen, Y.-R. Zhang, Y. Wu, Y. Ye, C. Zha, S. Li, S. Guo *et al.*, Observation of thermalization and information scrambling in a superconducting quantum processor, *Phys. Rev. Lett.* **128**, 160502 (2022).
- [32] E. Orignac and T. Giamarchi, Meissner effect in a bosonic ladder, *Phys. Rev. B* **64**, 144515 (2001).
- [33] A. Petrescu and K. L. Hur, Bosonic mott insulator with meissner currents, *Phys. Rev. Lett.* **111**, 150601 (2013).
- [34] Y. Jian, X. Qiao, J.-C. Liang, Z.-F. Yu, A.-X. Zhang, and J.-K. Xue, Stability and superfluidity of the Bose-Einstein condensate in a two-leg ladder with magnetic field, *Phys. Rev. E* **104**, 024212 (2021).
- [35] C.-M. Halati and T. Giamarchi, Bose-Hubbard triangular ladder in an artificial gauge field, *Phys. Rev. Res.* **5**, 013126 (2023).
- [36] X. Zhou, S. Jia, and X.-W. Luo, Spin-tensor Meissner currents of ultracold bosonic gases in an optical lattice, *Phys. Rev. A* **108**, 013304 (2023).
- [37] S. Daul and D. J. Scalapino, Frustrated Hubbard ladders and superconductivity in κ -BEDT-TTF organic compounds, *Phys. Rev. B* **62**, 8658 (2000).
- [38] P.-B. He, Q. Sun, P. Li, S.-Q. Shen, and W. M. Liu, Magnetic quantum phase transition of cold atoms in an optical lattice, *Phys. Rev. A* **76**, 043618 (2007).
- [39] K. Totsuka, P. Lecheminant, and S. Capponi, Semiclassical approach to competing orders in a two-leg spin ladder with ring exchange, *Phys. Rev. B* **86**, 014435 (2012).
- [40] J. Fan, X. Zhou, W. Zheng, W. Yi, G. Chen, and S. Jia, Magnetic order in a Fermi gas induced by cavity-field fluctuations, *Phys. Rev. A* **98**, 043613 (2018).
- [41] X. Zhou, X.-W. Luo, G. Chen, S. Jia, and C. Zhang, Quantum spiral spin-tensor magnetism, *Phys. Rev. B* **101**, 140412(R) (2020).
- [42] M. Mancini, G. Pagano, G. Cappellini, L. Livi, M. Rider, J. Catani, C. Sias, P. Zoller, M. Inguscio, M. Dalmonte, and L. Fallani, Observation of chiral edge states with neutral fermions in synthetic Hall ribbons, *Science* **349**, 1510 (2015).
- [43] B. K. Stuhl, H.-I. Lu, L. M. Ayccock, D. Genkina, and I. B. Spielman, Visualizing edge states with an atomic Bose gas in the quantum Hall regime, *Science* **349**, 1514 (2015).
- [44] S.-L. Zhang and Q. Zhou, Two-leg Su-Schrieffer-Heeger chain with glide reflection symmetry, *Phys. Rev. A* **95**, 061601(R) (2017).
- [45] K. Monkman and J. Sirker, Operational entanglement of symmetry-protected topological edge states, *Phys. Rev. Res.* **2**, 043191 (2020).

- [46] P. Sompet, S. Hirthe, D. Bourgund, T. Chalopin, J. Bibo, J. Koepsell, P. Bojović, R. Verresen, F. Pollmann, G. Salomon, C. Gross, T. A. Hilker, and I. Bloch, Realizing the symmetry-protected Haldane phase in Fermi-Hubbard ladders, *Nature (London)* **606**, 484 (2022).
- [47] Y. Kuno and Y. Hatsugai, $Z_2 \times Z_2$ symmetry and Z_4 Berry phase of bosonic ladders, *Phys. Rev. A* **108**, 013319 (2023).
- [48] I. Danshita, J. E. Williams, C. A. R. Sá de Melo, and C. W. Clark, Quantum phases of bosons in double-well optical lattices, *Phys. Rev. A* **76**, 043606 (2007).
- [49] I. Danshita, C. A. R. Sá de Melo, and C. W. Clark, Reentrant quantum phase transition in double-well optical lattices, *Phys. Rev. A* **77**, 063609 (2008).
- [50] H. Deng, H. Dai, J. Huang, X. Qin, J. Xu, H. Zhong, C. He, and C. Lee, Cluster Gutzwiller study of the Bose-Hubbard ladder: Ground-state phase diagram and many-body Landau-Zener dynamics, *Phys. Rev. A* **92**, 023618 (2015).
- [51] X. Qiao, X.-B. Zhang, Y. Jian, A.-X. Zhang, Z.-F. Yu, and J.-K. Xue, Quantum phases of interacting bosons on biased two-leg ladders with magnetic flux, *Phys. Rev. A* **104**, 053323 (2021).
- [52] A. Padhan, R. Parida, S. Lahiri, M. K. Giri, and T. Mishra, Quantum phases of constrained bosons on a two-leg Bose-Hubbard ladder, *Phys. Rev. A* **108**, 013316 (2023).
- [53] G. Pupillo, A. Griessner, A. Micheli, M. Ortner, D.-W. Wang, and P. Zoller, Cold atoms and molecules in self-assembled dipolar lattices, *Phys. Rev. Lett.* **100**, 050402 (2008).
- [54] A. V. Gorshkov, S. R. Manmana, G. Chen, J. Ye, E. Demler, M. D. Lukin, and A. M. Rey, Tunable superfluidity and quantum magnetism with ultracold polar molecules, *Phys. Rev. Lett.* **107**, 115301 (2011).
- [55] L. I. R. Gil, R. Mukherjee, E. M. Bridge, M. P. A. Jones, and T. Pohl, Spin squeezing in a Rydberg lattice clock, *Phys. Rev. Lett.* **112**, 103601 (2014).
- [56] Z. Lan, J. Minář, E. Levi, W. Li, and I. Lesanovsky, Emergent devil's staircase without particle-hole symmetry in Rydberg quantum gases with competing attractive and repulsive interactions, *Phys. Rev. Lett.* **115**, 203001 (2015).
- [57] Y. He, Z. Bai, Y. Jiao, J. Zhao, and W. Li, Superradiance-induced multistability in one-dimensional driven Rydberg lattice gases, *Phys. Rev. A* **106**, 063319 (2022).
- [58] M. Azuma, Z. Hiroi, M. Takano, K. Ishida, and Y. Kitaoka, Observation of a spin gap in SrCu_2O_3 comprising spin- $\frac{1}{2}$ quasi-1D two-leg ladders, *Phys. Rev. Lett.* **73**, 3463 (1994).
- [59] T. Hong, K. P. Schmidt, K. Coester, F. F. Awwadi, M. M. Turnbull, Y. Qiu, J. A. Rodriguez-Rivera, M. Zhu, X. Ke, C. P. Aoyama *et al.*, Magnetic ordering induced by interladder coupling in the spin- $\frac{1}{2}$ Heisenberg two-leg ladder antiferromagnet $\text{C}_9\text{H}_{18}\text{N}_2\text{CuBr}_4$, *Phys. Rev. B* **89**, 174432 (2014).
- [60] S. R. White, Density matrix formulation for quantum renormalization groups, *Phys. Rev. Lett.* **69**, 2863 (1992).
- [61] U. Schollwöck, The density-matrix renormalization group, *Rev. Mod. Phys.* **77**, 259 (2005).
- [62] G. Jotzu, M. Messer, F. Görg, D. Greif, R. Desbuquois, and T. Esslinger, Creating state-dependent lattices for ultracold fermions by magnetic gradient modulation, *Phys. Rev. Lett.* **115**, 073002 (2015).
- [63] J. Sebby-Strabley, M. Anderlini, P. S. Jessen, and J. V. Porto, Lattice of double wells for manipulating pairs of cold atoms, *Phys. Rev. A* **73**, 033605 (2006).
- [64] N. Henkel, R. Nath, and T. Pohl, Three-dimensional roton excitations and supersolid formation in Rydberg-excited Bose-Einstein condensates, *Phys. Rev. Lett.* **104**, 195302 (2010).
- [65] S. Ramanan, Tapan Mishra, Meetu Sethi Luthra, Ramesh V. Pai, and B. P. Das, Signatures of the superfluid-to-Mott-insulator transition in cold bosonic atoms in a one-dimensional optical lattice, *Phys. Rev. A* **79**, 013625 (2009).
- [66] T. Mishra, J. Carrasquilla, and M. Rigol, Phase diagram of the half-filled one-dimensional t-V-V' model, *Phys. Rev. B* **84**, 115135 (2011).
- [67] A. D. Greentree, C. Tahan, J. H. Cole, and L. C. L. Hollenberg, Quantum phase transition of light, *Nat. Phys.* **2**, 856 (2006).
- [68] J. Koch and K. L. Hur, Superfluid-Mott-insulator transition of light in the Jaynes-Cummings lattice, *Phys. Rev. A* **80**, 023811 (2009).
- [69] C.-W. Wu, M. Gao, Z.-J. Deng, H.-Y. Dai, P.-X. Chen, and C.-Z. Li, Quantum phase transition of light in a one-dimensional photon-hopping-controllable resonator array, *Phys. Rev. A* **84**, 043827 (2011).
- [70] T. Grujic, S. R. Clark, D. Jaksch, and D. G. Angelakis, Non-equilibrium many-body effects in driven nonlinear resonator arrays, *New J. Phys.* **14**, 103025 (2012).
- [71] F. Crépin, N. Laflorencie, G. Roux, and P. Simon, Phase diagram of hard-core bosons on clean and disordered two-leg ladders: Mott insulator-Luttinger liquid-Bose glass, *Phys. Rev. B* **84**, 054517 (2011).
- [72] A. J. Leggett, Bose-Einstein condensation in the alkali gases: Some fundamental concepts, *Rev. Mod. Phys.* **73**, 307 (2001).
- [73] J. Dalibard, F. Gerbier, G. Juzeliūnas, and P. Öhberg, Artificial gauge potentials for neutral atoms, *Rev. Mod. Phys.* **83**, 1523 (2011).